Electronic Supplementary Material (ESI) for Dalton Transactions.

Supporting Information for

Layered lanthanide phosphonates Ln(2-qpH)(SO_4)(H_2O)$_2$ (Ln = La, Ce, Pr, Nd, Sm): polymorphism and magnetic Properties

Xiu-Fang Ma, Dai Zeng, Chang Xu, Song-Song Bao, Li-Min Zheng*

†State Key Laboratory of Coordination Chemistry, School of Chemistry and Chemical Engineering, Collaborative Innovation Center of Advanced Microstructures, Nanjing University, Nanjing 210023, P. R. China.

*correspondence to: lmzheng@nju.edu.cn,

Contents

I. Literature review of Ce/Nd-based SMMs

Table S1 Literature review of Ce/Nd-based SMMs. Temperature dependence of the relaxation rate: $\tau^{-1}(T) = \tau_{QTM}^{-1} + AT + C\mathrm{Tn} + \tau_0^{-1}\exp(-U_{eff}/k_BT)$

	H (Oe)	U_{eff}/k_B (K)	τ_0 (s)	C ($K^{-n}s^{-1}$)	n	τ_{QTM}^{-1}(s^{-1})	A	Ref
Mononuclear compounds								
$[CeZn_2(L1)(AcO)_2]BPh_4$	250	37	2.7×10^{-7}					1
$[NdTp_3]$	100	4.1	5.5×10^{-5}					2
[Li(DME)3][Ce(COT″)2]	400	30	1.2×10^{-6}					3
$[Ce(NO_3)\{Zn(L1)(SCN)\}_2]$	1000	35.7	2.2×10^{-7}					4
$[Nd(NO_3)\{Zn(L1)(SCN)\}_2]$	1000	38.5	2.1×10^{-7}					4
$Na_9[Nd(W_5O_{18})_2]$	1000	73.9	3.6×10^{-10}					5
$[Li(DME)_3][Nd(COT'')_2]$	1000	21	5.5×10^{-5}					6
$[Ce^{III}\{Zn^{II}(L2)\}_2(MeOH)]BPh_4$	0	21.2	1.6×10^{-7}			3.8×10^{-4}		7
$[Ce(NO_3)_3(18\text{-c-}6)]$	1000	31.4	1.7×10^{-7}					8
	1000	30.3	2.2×10^{-7}	0.108	5(fixed)			
	1000	25.6	9.0×10^{-7}	16	9(fixed)			
$[Nd(NO_3)_3(18\text{-c-}6)]$	1000	29.9	2.9×10^{-9}					8
	1000	30.9	2.2×10^{-9}	4.1	5(fixed)			
	1000	33.4	1.6×10^{-9}	0.350	9(fixed)			
$[Ce(NO_3)_3(1,10\text{-diaza-}18\text{-c-}6)]$	1000	44	2.9×10^{-7}					8
	1000	45	2.2×10^{-7}	4.1	5(fixed)			
	1000	23	1.6×10^{-7}	0.350	9(fixed)			
$[Nd(NO_3)_3(1,10\text{-diaza-}18\text{-c-}6)]$	1000	69	2.1×10^{-6}					8
	1000	55	2.6×10^{-7}	0.050	5(fixed)			
	1000	73	1.4×10^{-6}	10.7	9(fixed)			
$[CeCd_3(Hquinha)_3(n\text{-}Bu_3PO)2I_3]\cdot3EtOH\cdot2H_2O$	1500	27	8.2×10^{-7}					9
$[NdL3(NO_3)_2]PF_6\cdot MeCN$	1000(O)	36	4.3×10^{-9}	4.1				10
	1000(R)				8.2			
	1000(O+R)	34	1.1×10^{-8}	2.8	5(fixed)			
	1000(O+R)	10	2.0×10^{-4}	0.081	9(fixed)			
$[L4Nd(H_2O_5]I_3\cdot L4(H_2O)$	0	16.08 24.68	2.6×10^{-4} 5.0×10^{-6}	16	9(fixed)			10
$Ce(fdh)_3(bpy)$	2000	33.3	1.8×10^{-7}					11
	2000(R)			0.4	6			
$Nd(fdh)_3(bpy)$	2000	28.8	9.2×10^{-8}					11
	200(R)			0.93	6.6			
$[L3Ce(NO_3)_3]$	200(R)	21.5	2.7×10-7					12
	200(R+D)			1.44	6.8		99.5	

$(NH_2Me_2)_3\{[Nd(Mo_4O_{13})$-$(DMF)_4]_3(BTC)_2\}\cdot 8DMF$	500	26.73	1.4×10^{-7}					13
$[Nd(CyPh_2PO)_2(H_2O)_5]I_3\cdot 2(CyPh_2PO)\cdot 3EtOH$	0(R+Q)				5.12		5.1	14
	200(R)				6.54			
$[Nd(CO_3)_4H_2O]^{5-}$ (C_1)	1500 (R)	30.7	1.1×10^{-7}					15
	1500(R+D)			0.89	6.08		125.89	
$[Nd(CO_3)_4H_2O]^{5-}$ (C_4)	1500 (R)	9.25	2.1×10^{-6}					15
$[Ce(dmso)_8][Ce(\eta_2\text{-}NO_3)_2(dmso)_4(\alpha\text{-}Mo_8O_{26})_{0.5}][Mo_6O_{19}]$	200	24.4	1.1×10^{-6}					16
$Cp^*_2Nd(BPh_4)$	1000	41.7	1.4×10^{-6}	0.0286	5.2		1.1	17
$[Nd(ntfa)_3(phen)]$	1500(O+R)	25.88	2.2×10^{-7}	135	2.4			18
$[Nd(ntfa)_3(5,5'\text{-}Me_2bipy)]$	1500 (O+R)	44.56	1.0×10^{-9}	186	3.0			18
$[Nd(ntfa)_3(4,4'\text{-}M_{t2}bipy)]$	1500 (O+R)	27.31	8.7×10^{-8}	59	2.3			18
Polynuclear compounds								
$[Nd_2(CNCH_2COO)_6(H_2O)_4]\cdot 2H_2O$	1500	26.6	1.8×10^{-7}					19
$K_{14}Na_6H_4[\{(As_2W_{19}O_{67}(H_2O))Nd(H_2O)_2\}_2(C_2O_4)]\cdot 64H_2O$	500	6.78	5.5×10^{-12}					20
$[Nd_2(2\text{-}FBz)_4(NO_3)_2(phen)_2]$	1500	13.67	7.4×10^{-6}	0.02	9		265.21	21
$[Nd_2(\mu_2\text{-}9\text{-}AC)_4(9\text{-}AC)_2(bpy)_2]$	4000(R)	11.5	7.5×10^{-6}					22
	4000(R+D)			1.03	6		823.60	
$[Nd_2(L)_4(H_2O)_6](L5)_2(H_2O)_{14}$	1200	21.2	1.6×10^{-7}			3.8×10^{-4}		23
$[Nd^{III}_4(H_2O)_{17}(pzdo)_5][Mo^{IV}(CN)_8]_3\}9H_2O$	1500(R)			312	2.99			24
$[Nd^{III}_6(\mu_3\text{-}OH)(\mu_3\text{-}\eta^2\text{-}Form)_6(Form)_2(NO_3)_2(BMPC)_3(H_2O)_2]$	3000	3.4	3.1×10^{-4}					25
1D compounds								
$\{[Nd(\mu_2\text{-}L5)_3(H_2O)_2]\cdot MeCN\}_n$	2000	27	4.1×10^{-7}					26
$[Nd(\mu_2\text{-}L6)(L6)(CH_3COO)(H_2O)_2]_n$	3500	29	3.1×10^{-7}					26
$[Nd(\mu_2\text{-}L5)_3(H_2O)_2]\cdot H_2O$	2000	28(2)	7.3×10^{-7}					27
$[Nd(\mu_2\text{-}L6)_2(CH_3COO)(H_2O)_2]_n$	2000	19.7	3.4×10^{-7}					27
$\{[Nd(pzdo)(H_2O)_4][Co(CN)_6]\}\cdot 0.5(pzdo)\cdot 4H_2O$	1000	51	4.5×10^{-8}	0.09	5.6	2.2		28
$[Nd(\alpha\text{-}fur)_3(H_2O)_2]_n$	1200	121	1.0×10^{-13}	141	3.7	350	1900	29
$\{Nd_{0.065}La_{0.935}(\alpha\text{-}fur)_3(H_2O)_2\}_n$	1200	61	3.6×10^{-11}	2.9×10^{-3}	9.9	7.82	0.25	29

L1 = 6,6′-(ethane-1,2-diylbis(azanylylidene))bis(methanylylidene)bis(2-methoxyphenol); Tp^- = trispyrazolylborate; DME = dimethoxyethane; COT″ = 1,4-bis(trimethylsilyl)cyclooctatetraenyldianion; L2 = 6,6′-(2,2-dimethylpropane-1,3-diyl)bis(azan-1-yl-1-

ylidene)bis(methan-1-yl-1-ylidene) bis(2-methoxyphenol); 18-Crown-6 = 1,4,7,10,13,16-hexaoxacyclooctadecane; 1,10-diaza-18-crown-6 = 1,4,10,13-tetraoxa-7,16-diazacyclooctadecane； H_2quinha = quinaldichydroxamic acid; L3 = a helical hexa-dentate; L4 = tBuPO(NHiPr)2; fdh = 1,1,1-fluoro-5,5-dimethyl-hexa-2,4-dione; bpy = 2,2'-bipyridine; dmso = dimethylsulfoxide；Tp^- = trispyrazolylborate; H_2FBz = 2-fluorobenzoic acid; phen = 1,10-phenanthroline; H_2FBz = 2-fluorobenzoic acid; phen = 1,10-phenanthroline; L5 = 2,6-dioxo-5-[(2,4,6-trioxo-5-hexahydropyrimi-dinylidene)amino]-3H-pyrimidin-4-olate); pzdo = pyrazine-N,N'-dioxide; BMPC = (9E)-N′-(1-(6-((E)-1-(5-(pyridine-2-yl)-1H-pyrazole-3-carboylimino)ethyl)pyridin-2-yl)-ethenamine)-3-(pyridine-2-yl)-1H-pyrazole-5-carbohydrazide; L5 = 3,5-dinitrobenzoic acid; L6 = 2,4-dinitrobenzoic acid; pzdo = pyrazine-N,N'-dioxide; pzdo = pyrazine-N,N'-dioxide; *α*-fur = C_4H_3OCOO.

II. Primary characterization

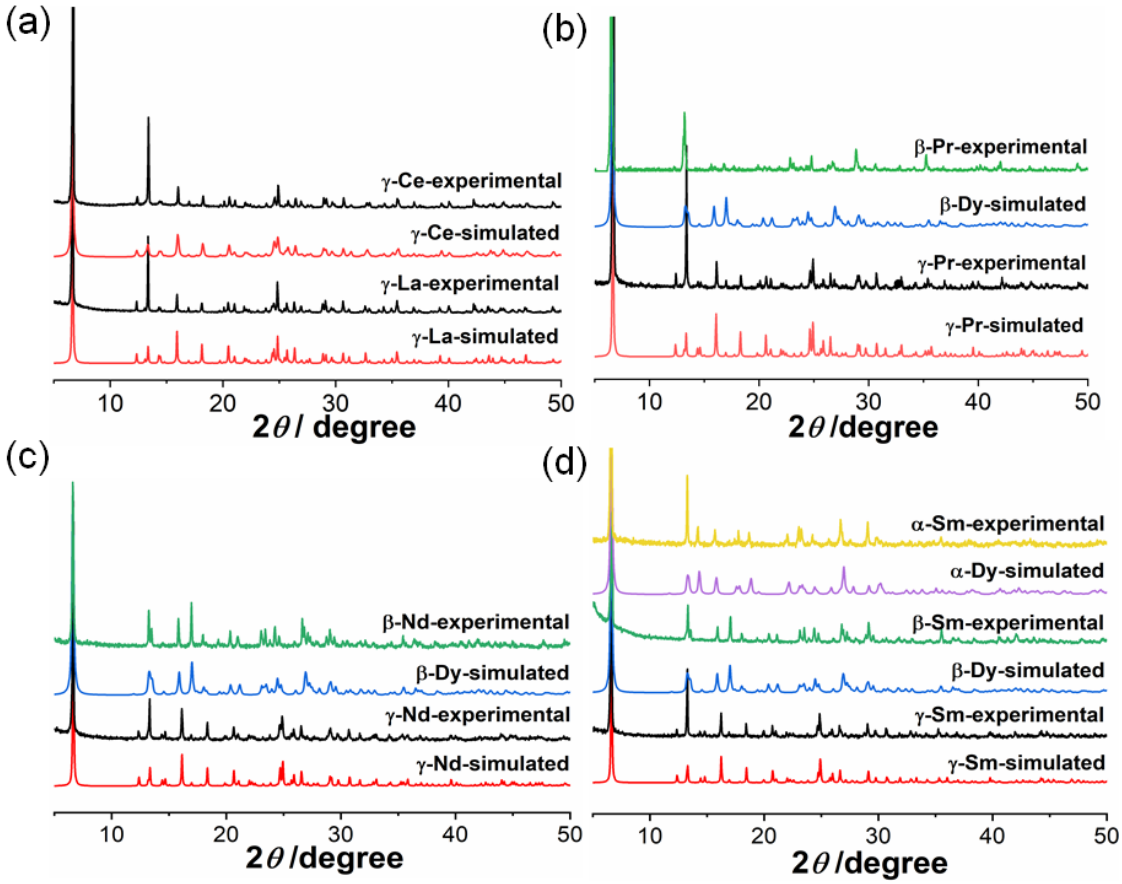

Figure S1. The powder XRD patterns for compounds **γ-La**, **γ-Ce** (a), **β-Ln** and **γ-Ln** [Ln = Pr (b), Nd (c)], **α-Sm**, **β-Sm** and **γ-Sm** (d). The patterns simulated from the single crystal data are also given. Since single crystal data of **α-Ln** and **β-Ln** are not available, the pattern simulated from the single crystal data of **α-Dy** and **β-Dy** are presented in for comparison.

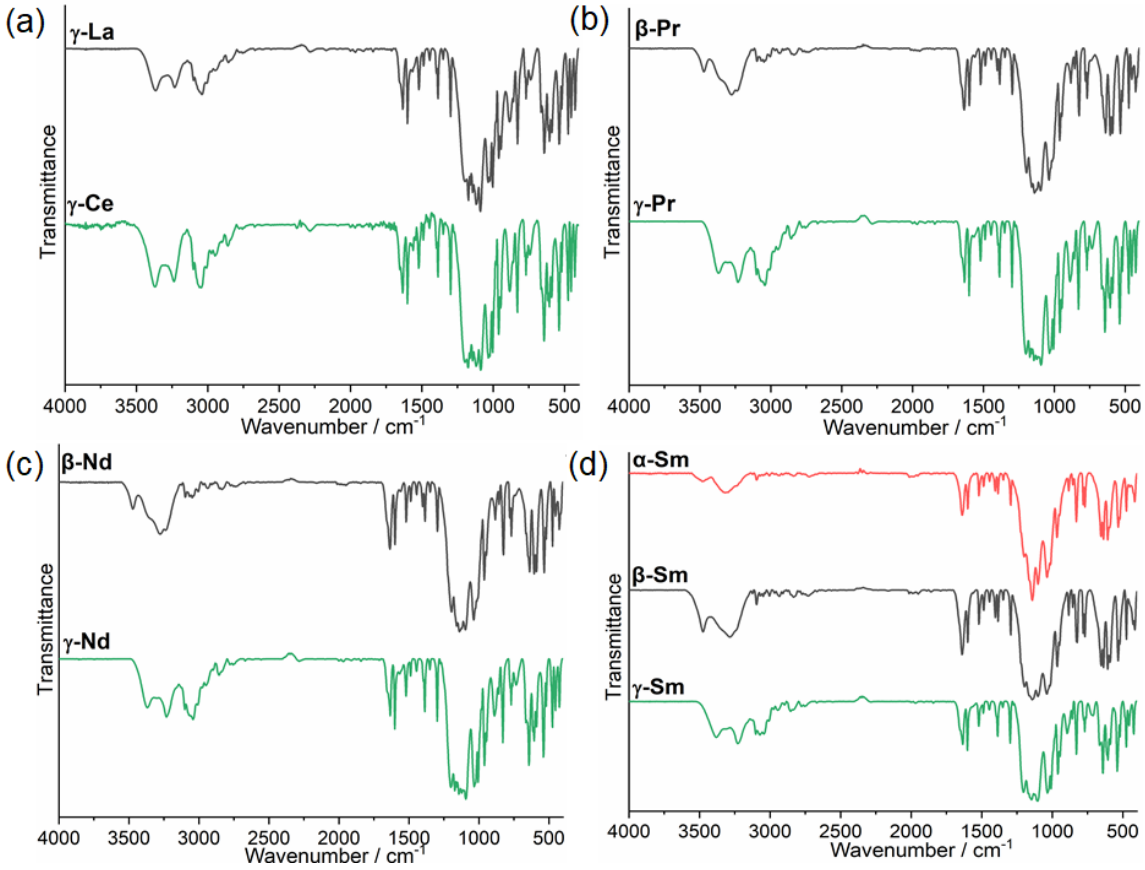

Figure S2. IR plots for compounds **γ-La**, **γ-Ce** (a), **β-Ln** and **γ-Ln** [Ln = Pr (b), Nd (c)], **α-Sm**, **β-Sm** and **γ-Sm** (d).

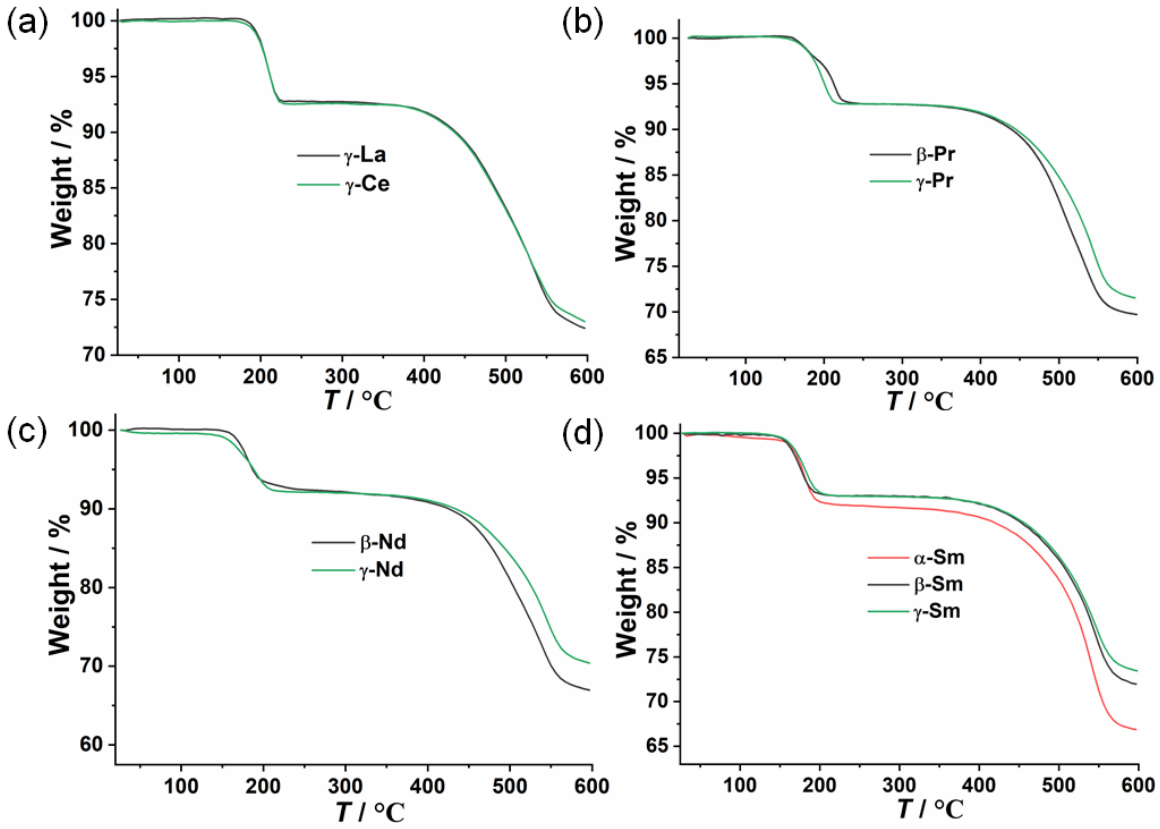

Figure S3. TG plots for complexes compounds **γ-La**, **γ-Ce** (a), **β-Ln** and **γ-Ln** [Ln = Pr (b), Nd (c)], **α-Sm**, **β-Sm** and **γ-Sm** (d). The weight losses in the temperature range 25-250 ºC are 7.4 % for La (calcd. 7.5 %), 7.5 % for Ce (calcd. 7.5 %), 7.4 % for Pr (calcd. 7.5 %), 7.5% for Nd (7.4 %), and 7.4 % for **α-Sm** and 7.2% for **β-Sm** and **γ-Sm** (calcd. 7.3 %).

III. Crystal structures

Table S2. Crystallographic data for **γ-Ln**.

	γ-La	**γ-Ce**	**γ-Pr**	**γ-Nd**	**γ-Sm**
Empirical Formula	$C_9H_{11}LaNO_9PS$	$C_9H_{11}CeNO_9PS$	$C_9H_{11}PrNO_9PS$	$C_9H_{11}NdNO_9PS$	$C_9H_{11}SmNO_9PS$
Fw	479.13	480.34	481.13	484.46	490.60
crystal system	Orthorhombic	Orthorhombic	Orthorhombic	Orthorhombic	Orthorhombic
Space group	Pbca	Pbca	Pbca	Pbca	Pbca
a (Å)	8.5067(19)	8.4923(11)	8.4758(18)	8.4677(19)	8.4635(7)
b (Å)	12.250(3)	12.1763(15)	12.107(3)	12.060(3)	11.9568(11)
c (Å)	26.474(6)	26.509(3)	26.511(6)	26.514(6)	26.595(2)
V (Å^3), Z	2758.8(11), 8	2741.1(6),8	2720.4(10),8	2707.5(10), 8	2691.4(4), 8
D_c (g cm^{-3})	2.307	2.328	2.349	2.377	2.421
F (000)	1856	1864	1872	1880	1896
μ (mm^{-1})	3.412	3.638	3.901	4.156	4.687
reflns collected	13735	13788	13618	13512	13442
unique reflns	2700	2698	2676	2667	2650
R_{int}	0.0438	0.0896	0.0379	0.0423	0.0367
GOF on F^2	1.074	1.029	1.198	1.271	1.218
R_1,wR_2 [I>2σ(I)] [a]	0.0544, 0.0939	0.0609, 0.1195	0.0375, 0.0748	0.0417, 0.0817	0.0314, 0.0689
R_1,wR_2 (all data) [a]	0.0614, 0.0969	0.0913, 0.1328	0.0430, 0.0769	0.0453, 0.0832	0.0333, 0.0697
CCDC number	2233015	2233016	2233020	2233021	2233022

[a] $R_1 = \Sigma||F_o|-|F_c||/\Sigma|F_o|$. $wR_2=[\Sigma w(F_o^2-F_c^2)^2/\Sigma w(F_o^2)^2]^{1/2}$

Table S3. Selected bond lengths (Å) and angles (º) for **γ-Ln**.

	***γ*-La**	***γ*-Ce**	***γ*-Pr**	***γ*-Nd**	***γ*-Sm**
Ln1-O1	2.501(5)	2.469(7)	2.445(4)	2.423(4)	2.385(3)
Ln1-O4	2.573(5)	2.553(6)	2.535(4)	2.522(4)	2.500(3)
Ln1-O5	2.636(5)	2.608(6)	2.582(4)	2.563(4)	2.523(3)
Ln1-O2A	2.472(5)	2.425(7)	2.404(4)	2.381(4)	2.330(4)
Ln1-O3B	2.406(5)	2.368(6)	2.354(3)	2.345(4)	2.310(4)
Ln1-O5C	2.612(5)	2.586(6)	2.572(3)	2.557(4)	2.526(3)
Ln1-O1W	2.488(5)	2.471(7)	2.441(4)	2.423(4)	2.394(3)
Ln1-O2W	2.593(5)	2.582(6)	2.560(4)	2.549(4)	2.530(3)
O1-Ln1-O1W	81.10(18)	81.2(2)	80.41(12)	80.06(14)	79.36(12)
O1-Ln1-O2W	90.91(17)	89.8(2)	89.25(12)	88.66(14)	86.60(12)
O1-Ln1-O4	144.21(17)	145.0(2)	145.02(12)	145.26(15)	145.95(11)
O1-Ln1-O5	146.63(17)	147.0 (2)	147.47(11)	147.83(13)	148.78(11)
O1-Ln1-O2A	116.58(16)	115.9(2)	115.34(13)	114.65(15)	113.24(12)
O1-Ln1-O3C	79.52(18)	80.5(2)	81.27(12)	81.83(14)	83.81(12)
O1-Ln1-O5A	82.71(16)	82.6(2)	82.74(11)	82.67(12)	82.78(10)
O1W-Ln1-O2W	136.28(17)	135.3(2)	134.42(11)	133.61(13)	131.66(11)

O1W-Ln1-O4	69.60(18)	69.7(2)	70.15(12)	70.38(15)	70.92(11)
O1W-Ln1-O5	123.14(17)	123.8(2)	124.66(12)	125.28(13)	126.40(11)
O1W-Ln1-O2B	75.08(18)	75.2(2)	74.92(13)	74.77(15)	74.55(12)
O1W-Ln1-O3C	74.50(18)	75.2(2)	75.79(12)	76.42(14)	77.61(12)
O1W-Ln1-O5A	149.64(17)	150.1(2)	149.98(11)	150.05(13)	150.43(11)
O2W-Ln1-O4	124.45(17)	124.6(2)	124.86(12)	124.96(13)	125.69(11)
O2W-Ln1-O5	85.39(16)	85.22(19)	85.66(11)	85.75(13)	86.60(10)
O2W-Ln1-O3C	146.25(17)	146.4(2)	146.40(12)	146.39(13)	146.60(11)
O2W-Ln1-O2B	70.42(17)	69.8(2)	69.88(12)	69.56(14)	69.17(12)
O2W-Ln1-O5A	69.27(16)	69.44(19)	69.60(10)	69.79(12)	69.89(10)
O4-Ln1-O5	53.68(16)	54.22(19)	54.61(11)	54.98(12)	55.53(10)
O4-Ln1-O2B	75.94(17)	75.6(2)	75.32(12)	75.22 (14)	74.82(12)
O4-Ln1-O3C	73.31(18)	73.7 (2)	73.67(12)	73.98(13)	74.06(11)
O4-Ln1-O5A	112.80(16)	113.50(19)	114.11(11)	114.74(12)	116.00(10)
O5-Ln1-O2B	93.41(17)	92.9(2)	92.93(12)	92.91(14)	92.55(12)
O5-Ln1-O3C	85.33(18)	85.6(2)	85.40(11)	85.49(13)	85.29(11)
O5-Ln1-O5A	64.96(18)	65.1(2)	65.37(12)	65.67(14)	66.28(12)
O2B-Ln1-O3C	142.53(17)	143.0(2)	142.92(12)	143.28(13)	143.49(12)
O3C-Ln1-O5A	77.41(17)	77.4(2)	77.23(11)	77.04(13)	77.19(11)
O2B-Ln1-O5A	135.28(17)	134.7(2)	135.02(12)	135.02(14)	134.63(12)

Symmetry transformations used to generate equivalent atoms for **γ-Ln**: A: 1-x,1-y,1-z; B: -x,1-y,1-z; C: 1/2+x,1/2-y,1-z.

Table S4. Continuous Shape Measure (CShM) analyses of dysprosium geometries for **γ-Ce** using the SHAPE2.1 Software.

Geometry	**γ-La**	**γ-Ce**	**γ-Pr**	**γ-Nd**	**γ-Sm**
Hexagonal bipyramid (D_{6h})	16.175	16.040	15.972	15.924	15.635
Cube (O_h)	12.124	12.074	12.046	12.014	11.895
Square antiprism (D_{4d})	3.237	3.156	3.093	3.049,	2.983
Triangular dodecahedron (D_{2d})	2.747	2.632	2.508	2.416	2.248
Johnson gyrobifastigium J26 (D_{2d})	13.556	13.289	13.222	13.125	12.812
Johnson elongated triangular (D_{3h})	24.986	25.074	25.325	25.486	25.869
Biaugmented trigonal prism J50 (C_{2v})	3.029	2.911	2.803	2.747	2.595
Biaugmented trigonal prism (C_{2v})	2.051	1.979	1.919	1.901	1.837
Snub diphenoid J84 (D_{2d})	4.390	4.188	4.078	3.971	3.728
Triakis tetrahedron (T_d)	2.051	12.670	12.641	12.637	12.565
Elongated trigonal bipyramid (D_{3h})	4.390	21.745	22.016	22.208	22.679

Table S5. Hydrogen bond lengths (Å) and angles (deg) for compound **γ-Ce**.

D-H···A	*d*(D-H) /Å	*d*(H···A)/Å	*d*(D···A)/Å	∠ DHA /°
N1-H1···O4^{i}	0.9100	1.9700	2.849(10)	163.00
O1W-H1Wa···O6^{ii}	0.9100	1.7800	2.679(9)	172.00
O1W-H1Wb···O2W^{iii}	0.9100	1.8400	2.725(9)	166.00
O2W-H2Wa···O1^{iv}	0.9100	1.8400	2.712(9)	160.00
O2W-H2Wb···O7^{v}	0.9000	1.7800	2.655(9)	163.00
C5-H5···O6^{i}	0.9300	2.5000	3.155(13)	127.00
C8-H8···O4^{i}	0.9300	2.5500	3.267(12)	134.00

Symmetry codes: i, -1/2+x,1/2-y,1-z; ii, 1/2-x,-1/2+y,+z; iii, -x,1-y,1-z, 1/2-z; iv, 1/2-x,1/2+y,+z; v, 1-x,1-y,1-z.

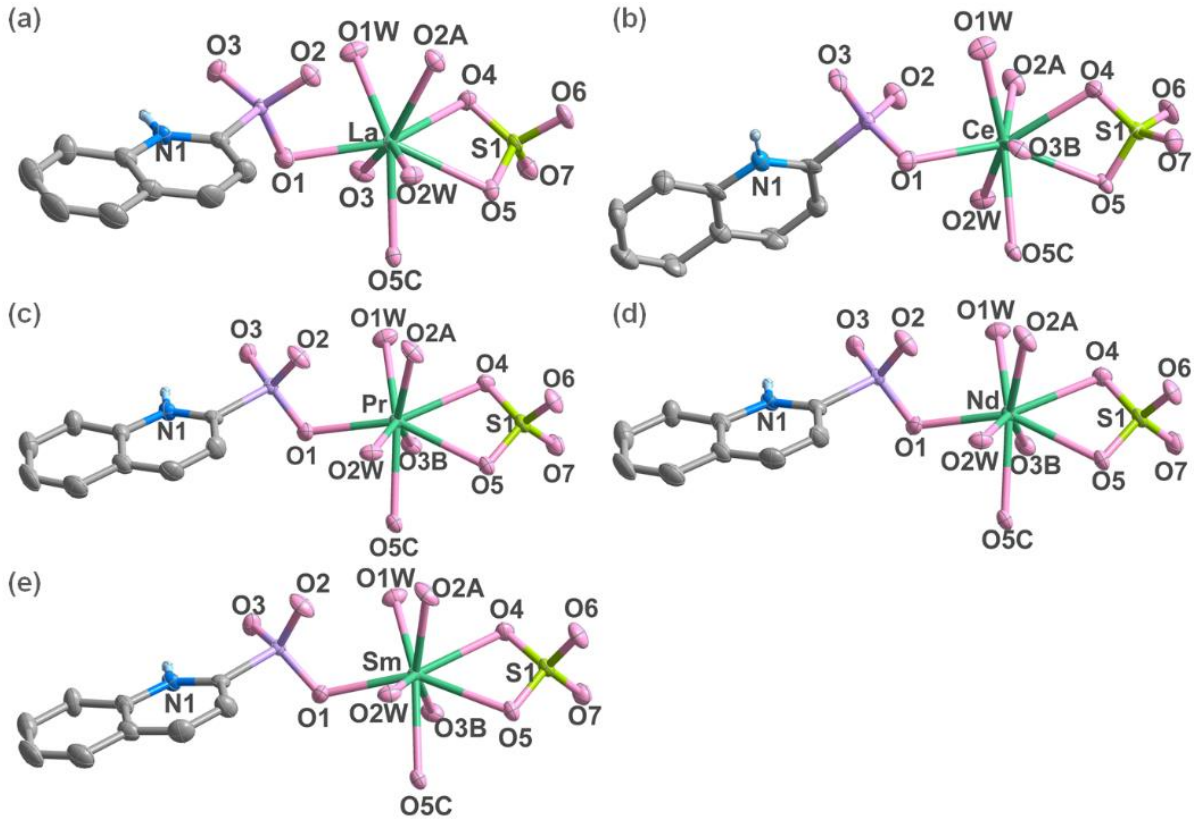

Figure S4. Building units of structures **γ-La (a), γ-Ce (b), γ-Pr (c), γ-Nd (d)** and **γ-Sm (e)** with an atomic labelling scheme (50% probability).

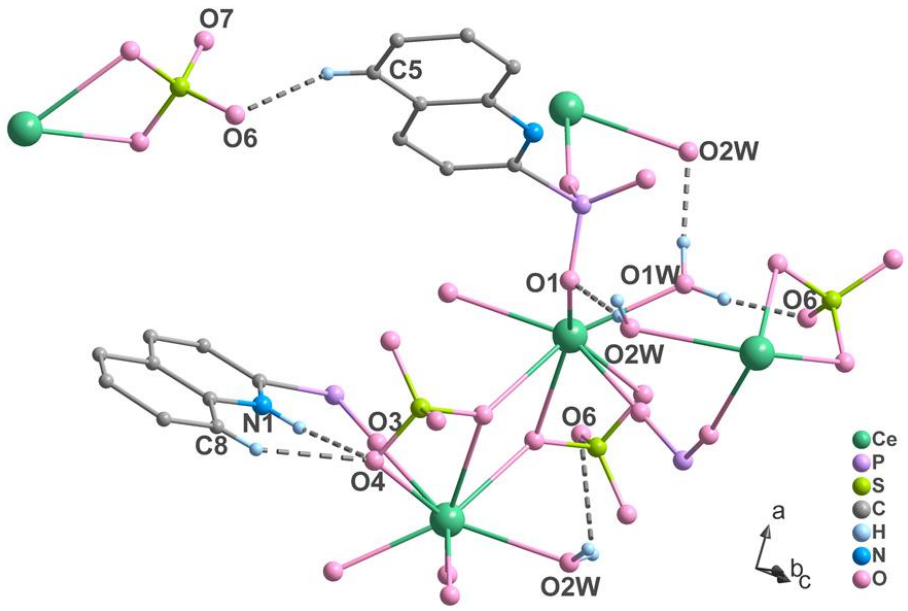

Figure S4. Intra- and inter-layer hydrogen-bond interactions for **γ-Ce**.

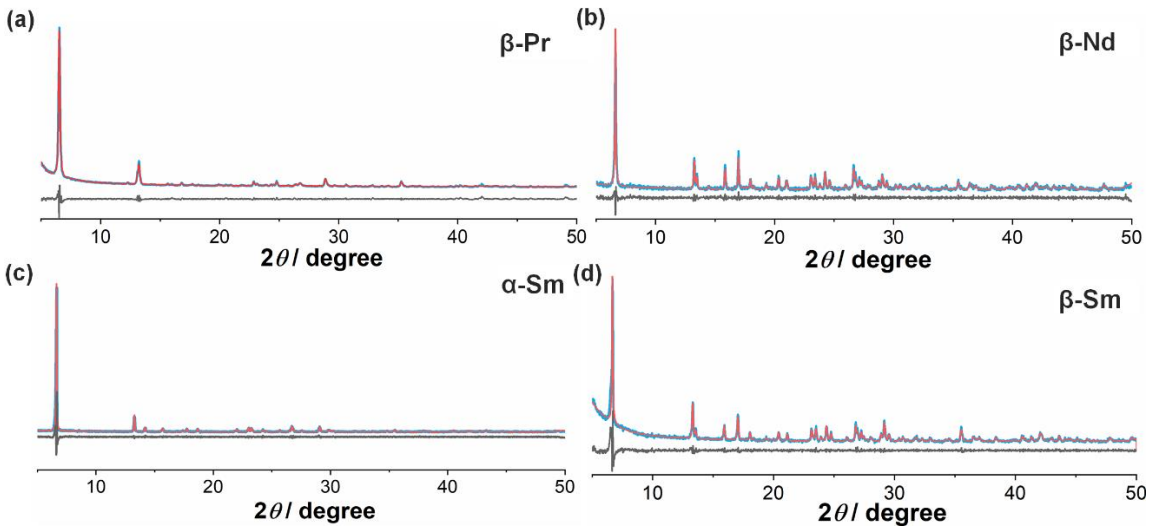

Figure S5 The PXRD pattern of **β-Pr** (a), **β-Nd** (b), **α-Sm** (c) and **β-Sm** (d) refined by TOPAS software to determine the unit cell.

Table S6. Crystallographic parameters of compounds **β-Pr, β-Nd, α-Sm** and **β-Sm** obtained by fitting with TOPAS software. Crystallographic parameters of **α-Dy** and **β-Dy** are presented in for comparison.

	α-Dy	**β-Dy**	**β-Pr**	**β-Nd**	**α-Sm**	**β-Sm**
crystal	monoclinic	triclinic	triclinic	triclinic	monoclinic	triclinic
Space	$P2_1/c$	$P\bar{1}$	$P\bar{1}$	$P\bar{1}$	$P2_1/c$	$P\bar{1}$
a (Å)	13.3163(5)	6.792(3)	6.08	6.85	13.33	6.83
b (Å)	6.7704(3)	7.596(4)	7.72	7.64	6.84	7.62
c (Å)	15.0967(6)	13.368(6)	13.61	13.41	15.25	13.38
α (deg)	90	90.362(8)	90.92	90.32	90	90.33
β (deg)	90.6391(6)°	93.280(7)	93.24	93.12	90.72	93.15
γ (deg)	90	102.383(7)	101.66	102.00	90	102.10
V (Å^3)	1360.98(10)	672.4(5)	624.25	686.57	1390.63	679.77
*R*wp (%)	-	-	10.9	8.5	12.4	7.9

IV. Magnetic studies

Table S7 The parameters obtained by fitting the ac magnetic susceptibilities for **γ-Ce** under different dc fields at 2K.

Field / Oe	χ_T / cm^3 mol^{-1}	χ_S / cm^3 mol^{-1}	ln(τ / s)	α	*R*esidual
500	0.13	0.09	-7.72	0.14	1.3×10^{-4}
1000	0.13	0.05	-7.55	0.20	2.0×10^{-4}
1500	0.13	0.03	-7.38	0.22	1.2×10^{-4}
2000	0.13	0.02	-7.34	0.23	1.7×10^{-4}
2500	0.12	0.02	-7.34	0.25	1.3×10^{-4}
3000	0.12	0.01	-7.30	0.25	2.0×10^{-4}

Table S8 The parameters obtained by fitting the ac magnetic susceptibilities for **β-Nd** under different dc fields at 2K.

Field / Oe	χ_T / cm^3 mol^{-1}	χ_S / cm^3 mol^{-1}	ln (τ / s)	α	*R*esidual
400	0.25	0.21	-7.73	0.08	3.3×10^{-4}
600	0.25	0.18	-7.60	0.18	2.8×10^{-4}
800	0.25	0.14	-7.51	0.26	3.2×10^{-4}
1000	0.25	0.11	-7.38	0.30	4.3×10^{-4}
1500	0.24	0.07	-7.16	0.31	3.0×10^{-4}
2000	0.24	0.05	-7.06	0.32	5.5×10^{-4}
2500	0.24	0.04	-7.01	0.35	2.2×10^{-3}
3000	0.23	0.04	-7.03	0.33	8.4×10^{-4}
3500	0.22	0.02	-7.04	0.43	1.9×10^{-3}
4000	0.21	0.03	-7.12	0.35	1.1×10^{-3}
4500	0.21	0.03	-7.22	0.36	1.2×10^{-3}
5000	0.11	0.07	-7.35	0.46	1.7×10^{-3}

Table S9 The parameters obtained by fitting the ac magnetic susceptibilities for **γ-Nd** under different dc fields at 2K.

Field / Oe	χ_T / cm^3 mol^{-1}	χ_S / cm^3 mol^{-1}	ln(τ / s)	α	*R*esidual
400	0.28	0.21	-7.51	0.04	9.1×10^{-4}
600	0.28	0.16	-7.59	0.02	5.9×10^{-4}
800	0.28	0.12	-7.47	0.05	1.5×10^{-3}
1000	0.27	0.09	-7.42	0.03	4.8×10^{-3}
1500	0.27	0.05	-7.28	0.05	9.5×10^{-4}
2000	0.26	0.04	-7.27	0.03	1.4×10^{-3}
2500	0.25	0.02	-7.30	0.06	2.5×10^{-3}
3000	0.25	0.01	-7.29	0.06	2.0×10^{-3}
3500	0.24	0.01	-7.38	0.09	2.3×10^{-3}
4000	0.23	7.79E-13	-7.48	0.13	5.3×10^{-3}
4500	0.22	1.15E-12	-7.59	0.09	2.3×10^{-3}
5000	0.20	1.66E-12	-7.67	0.10	2.7×10^{-3}

Table S10 The parameters obtained by fitting the χ_M" versus frequency data of compound **γ-Ce** under 2 kOe dc field.

T / K	χ_T / cm^3 mol^{-1}	χ_S / cm^3 mol^{-1}	ln(τ / s)	α	*R*esidual
2.2	0.11	0.02	-7.50	0.21	5.5×10^{-4}
2.4	0.11	0.02	-7.60	0.21	6.6×10^{-4}
2.6	0.10	0.02	-7.72	0.20	2.2×10^{-4}
2.8	0.09	0.02	-7.83	0.21	1.1×10^{-4}
3.0	0.09	0.02	-7.91	0.19	1.8×10^{-4}
3.2	0.08	0.02	-7.99	0.18	1.7×10^{-4}
3.4	0.08	0.03	-8.08	0.17	2.5×10^{-4}
3.6	0.07	0.03	-8.18	0.17	2.7×10^{-4}
3.8	0.07	0.03	-8.25	0.13	2.7×10^{-5}
4.0	0.07	0.03	-8.34	0.11	4.9×10^{-5}

Table S11 The parameters obtained by fitting the χ_M" versus frequency data of compound **β-Nd** under 2 kOe dc field.

T / K	χ_T / cm^3 mol^{-1}	χ_S / cm^3 mol^{-1}	ln(τ / s)	α	*R*esidual
1.8	0.33	0.09	-7.39	0.23	5.2×10^{-4}
2.0	0.30	0.10	-7.49	0.20	6.2×10^{-4}
2.2	0.27	0.10	-7.58	0.20	3.4×10^{-4}
2.4	0.25	0.10	-7.67	0.18	2.6×10^{-4}
2.6	0.23	0.09	-7.79	0.16	2.4×10^{-4}
2.8	0.22	0.09	-7.88	0.14	1.7×10^{-4}
3.0	0.21	0.09	-8.02	0.13	9.6×10^{-5}
3.2	0.19	0.09	-8.16	0.12	9.2×10^{-5}
3.4	0.18	0.09	-8.33	0.10	1.5×10^{-4}
3.6	0.17	0.09	-8.54	0.09	1.1×10^{-4}
3.8	0.16	0.09	-8.80	0.09	1.2×10^{-4}
4.0	0.16	0.09	-9.07	0.08	8.3×10^{-5}
4.2	0.15	0.08	-9.46	0.13	7.8×10^{-5}
4.4	0.14	0.08	-9.73	0.12	5.7×10^{-5}
4.6	0.14	0.08	-10.21	0.15	8.4×10^{-5}

Table S12 The parameters obtained by fitting the χ_M" versus frequency data of compound **γ**-Nd under 2 kOe dc field.

T / K	χ_T / cm^3 mol^{-1}	χ_S / cm^3 mol^{-1}	ln(τ / s)	α	*R*esidual
2.0	0.13	0.02	-7.36	0.04	3.1×10^{-4}
2.2	0.12	0.02	-7.56	0.05	2.8×10^{-4}
2.4	0.12	0.02	-7.76	0.06	1.5×10^{-4}
2.6	0.11	0.01	-7.97	0.05	2.3×10^{-4}
2.8	0.09	0.01	-8.19	0.07	1.5×10^{-4}
3.0	0.09	0.01	-8.42	0.07	3.2×10^{-5}
3.2	0.09	0.01	-8.57	0.06	1.3×10^{-5}
3.5	0.08	0.01	-8.92	0.05	1.5×10^{-4}
3.8	0.07	0.01	-9.10	0.02	1.7×10^{-4}
4.1	0.07	0.01	-9.58	0.02	1.2×10^{-5}
4.4	0.07	0.02	-9.83	0.03	1.0×10^{-5}

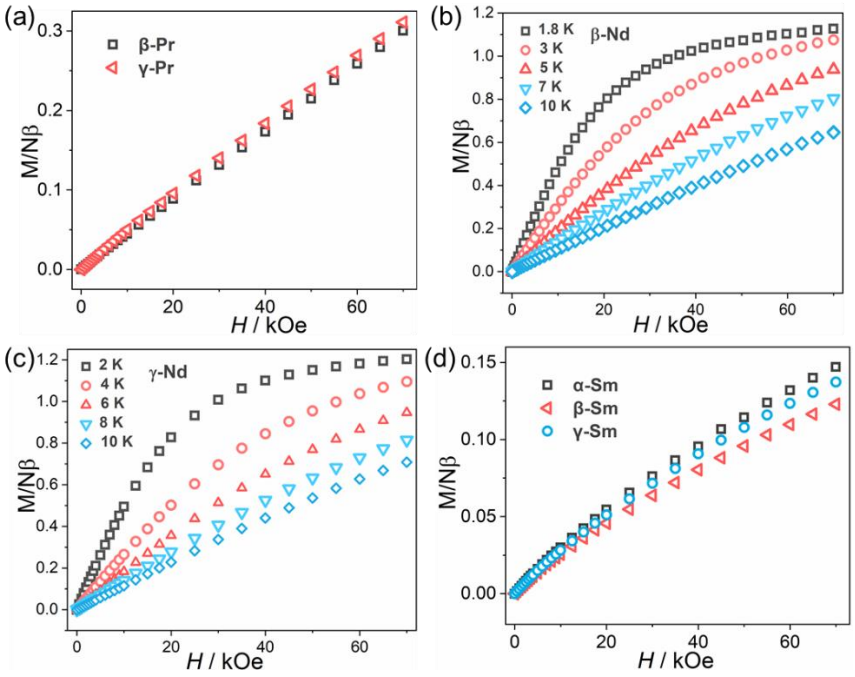

Figure S6. The isothermal magnetization for **β-Pr** and **γ-Pr** (a), **β-Nd**(b), **γ-Nd**(c), **α-Sm**, **β-Sm** and **γ-Sm**(d) as a function of *H* at depicted temperatures.

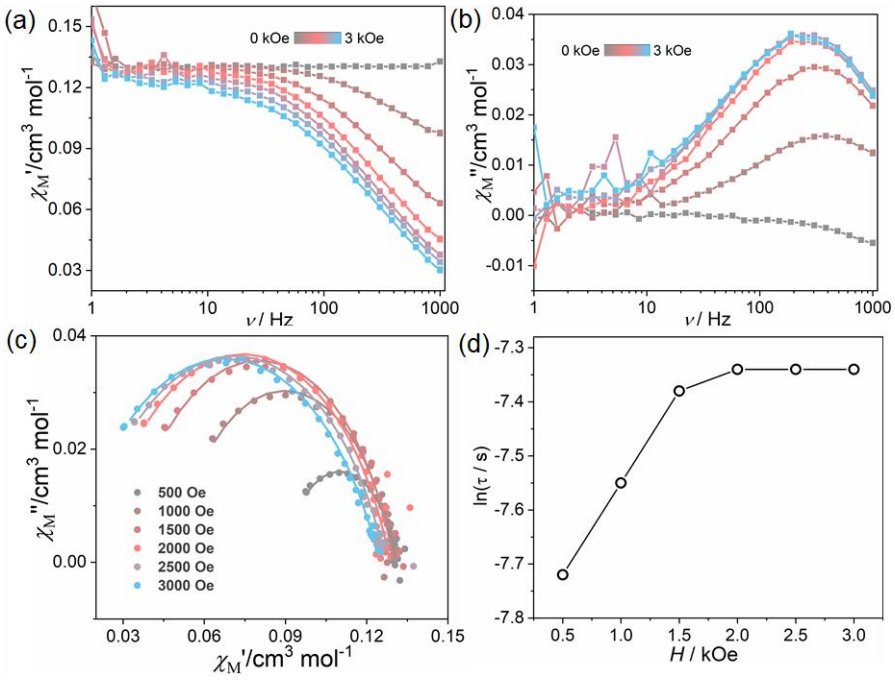

Figure S7. Frequency dependence of the χ_M' (a)andχ_M'' (b) signals of compound **γ-Ce** at 2 K under different *dc* fields; (b) Cole-Cole plots for **γ-Ce** obtained by using the *ac* susceptibility data at 2K under different fields; (c) Field dependent magnetic relaxation time at 2 K for **γ-Ce**. Solid lines are eye-guided.

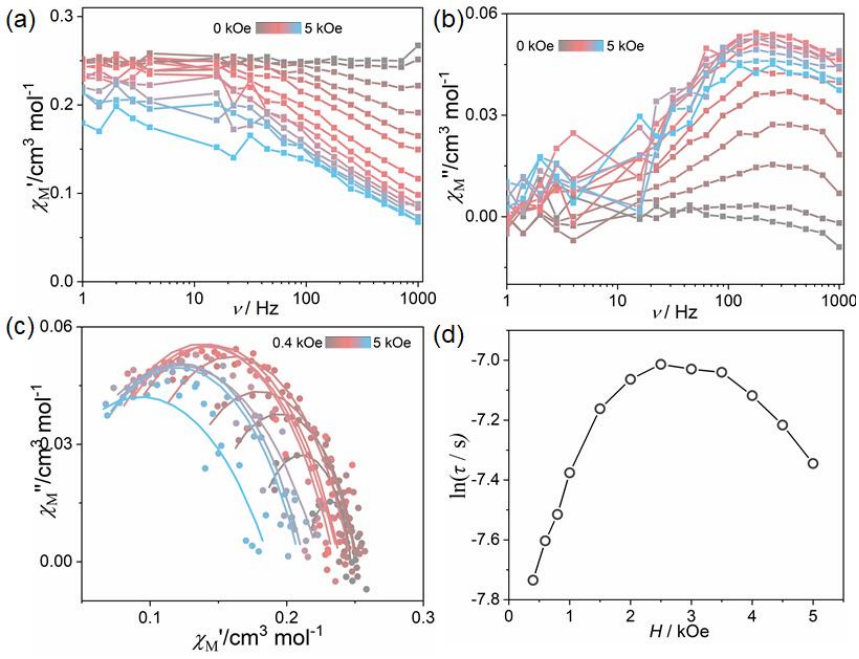

Figure S8. Frequency dependence of the χ_M' (a)andχ_M'' (b) signals of compound **β-Nd** at 2 K under different *dc* fields; (b) Cole-Cole plots for **β-Nd** obtained by using the *ac* susceptibility data at 2K under different fields; (c) Field dependent magnetic relaxation time at 2 K for **β-Nd**. Solid lines are eye-guided.

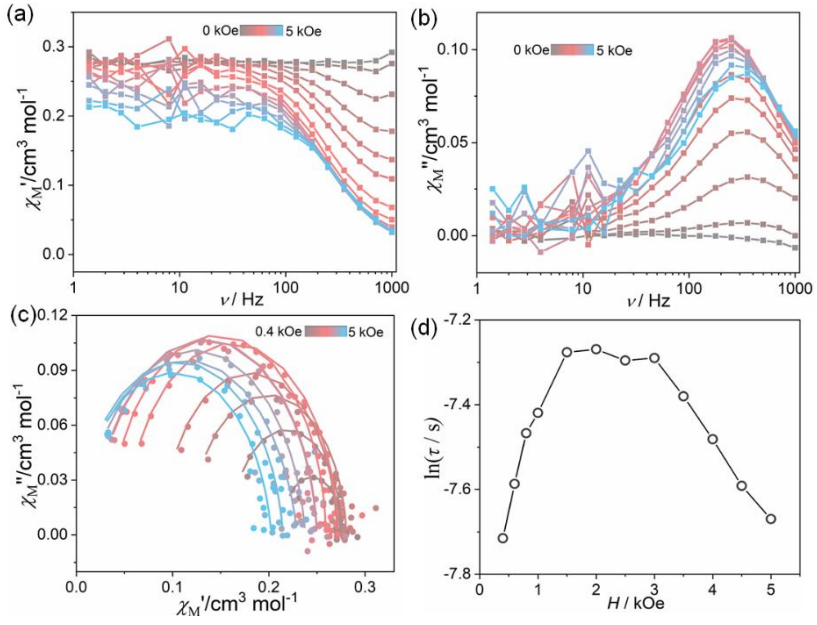

Figure S9. Frequency dependence of the χ_M' (a)andχ_M'' (b) signals of compound **γ-Nd** at 2 K under different *dc* fields; (b) Cole-Cole plots for **γ-Nd** obtained by using the *ac* susceptibility data at 2K under different fields; (c) Field dependent magnetic relaxation time at 2 K for **γ-Nd**. Solid lines are eye-guided.

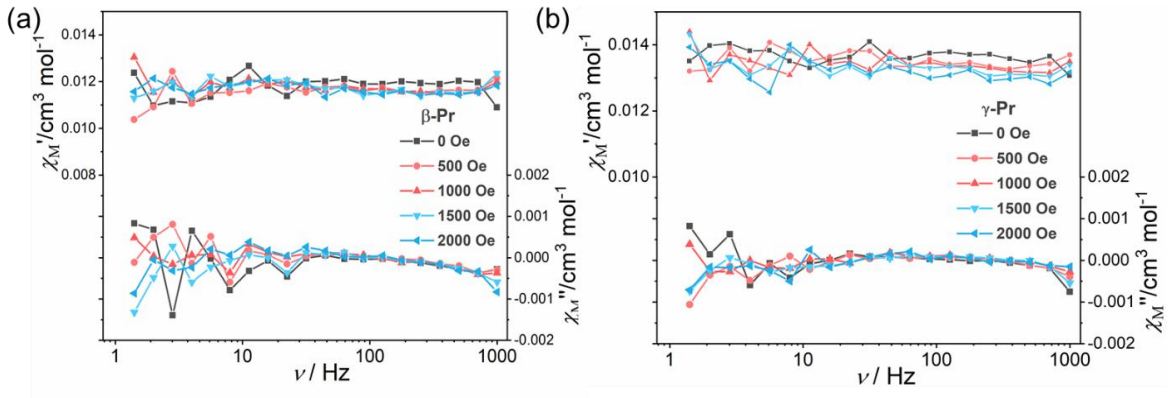

Figure S10. In-phase (χ') and out-of-phase (χ'') ac susceptibilities at depicted dc field for **β-Pr** (a) and **γ-Pr** (b).

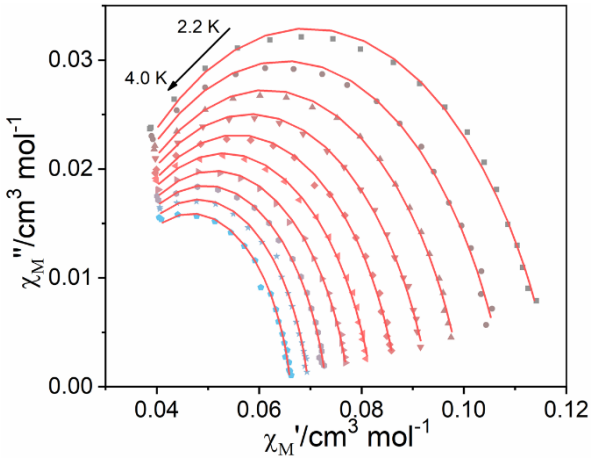

Figure S11. Cole-Cole plots for **γ-Ce** measured in the different temperatures range under 2 kOe dc field. The solid line represents the best fit using a generalized Debye model.

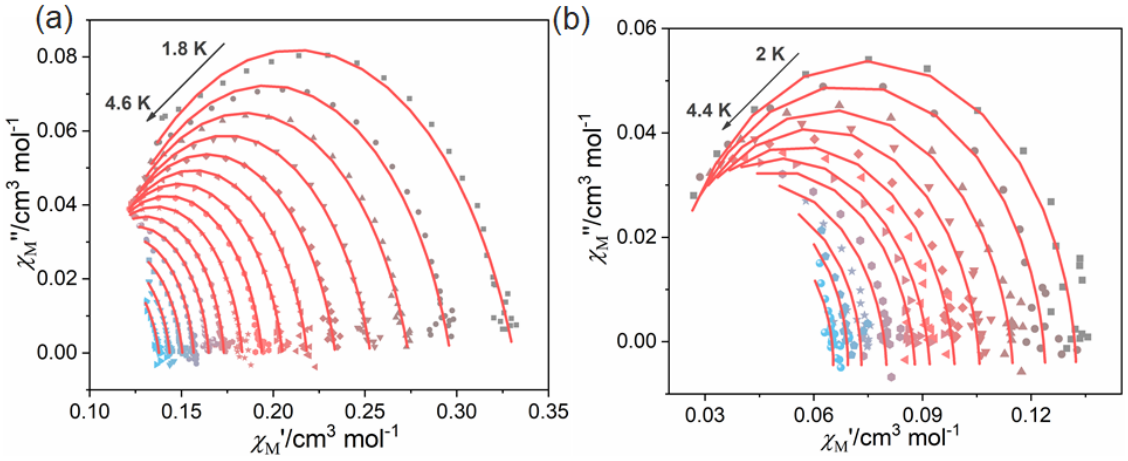

Figure S12. Cole-Cole plots for **β-Nd** (a) and **γ-Nd** (b) measured in the different temperatures range under 2 kOe dc field. The solid line represents the best fit using a generalized Debye model.

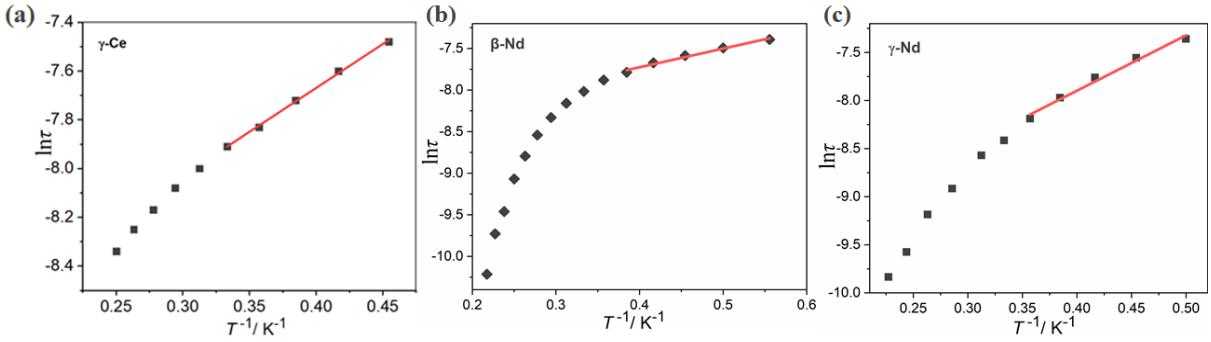

Figure S13. The ln(τ) vs. T^{-1} plots for **γ-Nd** (a)**, β-Nd** (b) and **γ-Nd** (c) fitted to the equation $\tau \sim [\exp(\hbar\omega\alpha/k_B T)]$.

V. References:

1 S. Hino, M. Maeda, K. Yamashita, Y. Kataoka, M. Nakano, T. Yamamura, H. Nojiri, M. Kofu, O. Yamamuro, T. Kajiwara, *Dalton Trans*. 2013, **42**, 2683–2686.

2 J. D. Rinehart and J. R. Long, *Dalton Trans*., 2012, **41**, 13572–13574.

3 J. J. Le Roy, l. Korobkov, J. E. Kim, E. J. Schelterb and M. Murugesu, *Dalton Trans*., 2014, **43**, 2737–2740.

4 C. Takehara, P. L. Then, Y. Kataoka, M. Nakano, T. Yamamurac and T. Kajiwara, *Dalton Trans*., 2015, **44**, 18276–18283.

5 J. J. Baldoví, J. M. Clemente-Juan, E. Coronado, Y. Duan, A. Gaita-Ariño and C. Gimenez-Saiz, *Inorg. Chem*. 2014, **53**, 9976-9980.

6 J. J. Le Roy, S. I. Gorelsky, I. Korobkov and M. Murugesu, *Organometallics* 2015, **34**, 1415-1418.

7 S. K. Singh, T. Gupta, L. Ungur and G. Rajaraman, *Chem. Eur. J.* 2015, **21**, 13812–13819.

8 H. Wada, S. Ooka, T. Yamamura and T. Kajiwara, *Inorg. Chem*., 2017, **56**, 147–155

9 Q.-W. Li, R.-C. Wan, Y.-C. Chen, J.-L. Liu, L.-F. Wang, J.-H. Jia, N. F. Chilton and M.-L. Tong, *Chem. Commun*., 2016, **52**, 13365-13368.

10 H. Wada, S. Ooka, D. Iwasawa, M. Hasegawa and T. Kajiwara, *Magnetochemistry* 2016, **2**, 43.

11 M.-X. Xu, Y.-S. Meng, J. Xiong, B.-W. Wang, S.-D. Jiang and S. Gao, *Dalton Trans*., 2018, **47**, 1966–1971.

12 S. K. Gupta, S. Shanmugan, T. Rajeshkumar, A. Borah, M. Damjanović, M. Schulze, W. Wernsdorfer, G. Rajaraman and R. Murugavel, *Dalton Trans*., 2019, **48**, 15928–15935.

13 H.-L. Zhang, X.-Y. Wu, J.-Z. Liao, X.-F. Kuang, W.-B. Yang and C.-Z. Lu, *Dalton Trans*., 2018, **47**, 1796–1800.

14 Y.-C. Chen, X.-S. Huang, J.-L. Liu and M.-L. Tong, *Inorg. Chem*. 2018, **57**, 11782−11787.

15 J. Li, L. Yin, S.-J. Xiong, X.-L. Wu, F. Yu, Z.-W. Ouyang, Z.-C. Xia, Y.-Q. Zhang, J. van Tol, Y. Song and Z.-X. Wang, *iScience* 2020, **23**, 100926.

16 A. Ben Khélifa, M. Salah Belkhiria, G. Huang, S. Freslon, O. Guilloub and K. Bernot, *Dalton Trans*., 2015, 44, 16458–16464.

17 S. Demir, K. R. Meihaus, J. R. Long, *J. organomet. Chem*, 2018, **857**, 164–169.

18 R. Vicente, A.Tubau, S. Speed, F. A. Mautner, F. Bierbaumer, R. C. Fischer and S. S. Massoud, *New J. Chem*., 2021, **45**, 14713–14723.

19 A. Arauzo, A. Lazarescu, S. Shova, E. Bartolomé, R. Cases, J. Luzón, J. Bartolomé and C. Turta, *Dalton Trans*., 2014, **43**, 12342–12356

20 H.-H. Chen, L. Sun, K.-T. Zheng, J.-P, Zhang, P.-T. Ma, J.-P. Wang and J.-Y. Niu, *Dalton Trans*., 2022, **51**, 10257–10265.

21 B. Casanovas, M. Font-Bardía, S. Speed, M. Salah El Fallah and R. Vicente, *Eur. J. Inorg. Chem*. 2018, 1928–1937.

22 B. Casanovas, S. Speed, O. Maury, M. Salah El Fallah, M. Font-Bardía and R. Vicente, *Eur. J. Inorg. Chem*. 2018, 3859–3867.

23 G. Huang, G. Calvez, Y. Suffren, C. Daiguebonne, S. Freslon, O. Guillou and K. Bernot, *Magnetochemistry* 2018, **4**, 44

24 R. Jankowski, J. J. Zakrzewski, M. Zychowicz, J. H. Wang, Y. Oki, S. Ohkoshi, S. Chorazy and B. Sieklucka, *J. Mater. Chem. C*, 2021, **9**, 10705–10717.

25 K. S. Das, S. Saha, B. Pal, A. Adhikary, S. Moorthy, S. Bala, S. Akhtar, P. K. Ghose, S. K. Singh, P. P. Ray and R. Mondal, *Dalton Trans*., 2022, **51**, 1617–1633.

26 A. Kaur Jassal, N. Aliaga-Alcalde, M. Corbella, D. Aravena, E. Ruiz and G. Hundal, *Dalton Trans*., 2015, **44**, 15774–15778.

27 A. Kaur Jassal, B. Singh Sran, Y. Suffren, K. Bernot, F. Pointillart, O. Cador and G. Hundal, *Dalton Trans.*, 2018, **47,** 4722–4732.

28 S. Chorazy, T. Charytanowicz, J. Wang, S. Ohkoshi and B. Sieklucka, *Dalton Trans*., 2018, **47**, 7870–7874.

29 E. Bartolomé, A. Arauzo, J. Luzón, S. Melnic, S. Shova, D. Prodius, I. C. Nlebedim, F. Bartoloméand J. Bartolomé, *Dalton Trans.*, 2019, **48**, 15386–15396.